# Structure−Property Relationships of the 10H Hexagonal-Type Perovskite $BaMn_{0.4}Fe_{0.6}O_{2.73}$

Laura Miranda,[†] Khalid Boulahya,[†] Aurea Varela,[†] José M. González-Calbet,[†] Marina Parras,*[,†] María Hernando,[†,‡] M. Teresa Fernández-Díaz,[‡] Antonio Feteira,[§] and Derek C. Sinclair[§]

*Departamento de Química Inorgánica, Facultad de Químicas, Universidad Complutense de Madrid, E-28040-Madrid, Spain, Institut Laue Langevin, BP 156X, F-38042 Grenoble, France, and Department of Engineering Materials, University of Sheffield, Mappin Street, Sheffield, S1 3JD, United Kingdom*

*Received March 7, 2007. Revised Manuscript Received May 7, 2007*

The crystal structure of $BaMn_{0.4}Fe_{0.6}O_{2.73}$, a recently identified oxygen-deficient 10H-type hexagonal perovskite in the system $BaMn_{1-x}Fe_xO_{3-y}$, has been established by a combination of electron microdiffraction and neutron diffraction. The structure (space group $P6_3/mmc$, $a = 5.74435(5)$ Å, and $c = 24.0331(3)$ Å) can be described by a stacking sequence $(hch'ch)_2$ along the *c*-axis with the anion deficiency located exclusively in the h′-$BaO_3$-type layers. The anion distribution in the h′-$BaO_3$ layers differs significantly from that observed for 10H $BaFeO_{2.8}$ and results in a 70:30 random distribution of corner-sharing tetrahedral $Fe_2O_7$ dimers and face-sharing octahedral $(Mn,Fe)_2O_9$ dimers as opposed to the exclusive $Fe_2O_7$ dimers in 10H $BaFeO_{2.8}$. The difference is attributed to the preference of Mn for octahedral coordination. The compound is a "leaky" insulator at room temperature with a permittivity of ∼20. The conduction mechanism has low activation energy, ∼0.3 eV, and is consistent with polaronic hopping associated with the Fe and/or Mn ions.

## Introduction

The perovskite structure of ideal formula $ABO_3$ can be regarded as resulting from the stacking of pseudo-close-packed $AO_3$ layers with B cations occupying one-quarter of the octahedral holes. When all the $AO_3$ layers stack in a cubic close-packed (ABC) sequence, c-$AO_3$, the $BO_6$ octahedra form the three-dimensional corner-sharing $BO_3$ network of the well-known cubic perovskite (3C structure-type). Conversely, if all the $AO_3$ layers are in a hexagonal close-packed (AB) sequence, h-$AO_3$, the $BO_6$ octahedra share faces and form infinite one-dimensional chains along the *c*-axis, which is referred to as the 2H structure-type hexagonal perovskite. Varying the ratio and the stacking sequence of the c- and h-$AO_3$ layers leads to different hexagonal polytypes in which the coordination polyhedra around the B sites can link together by sharing either a common face (h) or common corner (c). Many factors influence the stability of a particular polytype for a given composition, including the relative sizes of the A and B cations, the electronic configuration of the B cations and the oxygen content.

Recently, we have been investigating polytypism and oxygen deficiency in the $BaMn_{1-x}Fe_xO_{3-y}$ system and have reported the chemical composition and basic crystal structure of a new hexagonal perovskite with $x = 0.6$ and $y = 0.27$ that, according to XRD data, adopts a 10H-type structure with a $(hchch)_2$ stacking sequence, Figure 1 a.[1] This polytype can also be stabilized in both $BaFeO_{3-y}$ and $BaMnO_{3-y}$ systems. The structure of 10H-$BaFeO_{2.80}$, determined using single-crystal X-ray diffraction,[2] is closely related to the stoichiometric 10H $ABO_3$ polytype, but to fulfill the chemical composition, there are two oxygen deficient hexagonal h′-$BaO_2$ layers per unit cell in a $(hch'ch)_2$ sequence. The remaining two oxygen atoms are arranged in such a way that only one of them is within bonding distance of the two iron atoms adjacent to the layer, giving rise to the formation of two corner-sharing tetrahedra, Figure 1b. In the h′-$BaO_2$ layers, the barium and oxygen atoms are displaced from hexagonal special positions and lower the symmetry from hexagonal to orthorhombic. Moreover, additional oxygen deficiency can be tolerated up to a limiting composition of $BaFeO_{2.60}$; these additional vacancies are randomly distributed over the h-$BaO_3$ layers.[3]

Although our previous XRD study on a sample with composition $BaMn_{0.4}Fe_{0.6}O_{2.73}$[1] has shown this compound to adopt a 10H-type structure, the data did not permit elucidation of details concerning the cation arrangement, anion vacancy distribution and/or subtle changes in symmetry. Here, we provide a more detailed structural characterization of $BaMn_{0.4}Fe_{0.6}O_{2.73}$ from electron microdiffraction and neutron diffraction data. From these, the structural charac-

* Corresponding author. E-mail: mparras@quim.ucm.es. Fax: (34) 91 394 43 52.
[†] Universidad Complutense de Madrid.
[‡] Institut Laue Langevin.
[§] University of Sheffield.

(1) Miranda, L.; Ramírez-Castellanos, J.; Hernando, M.; Varela, A.; González-Calbet, J.; Parras, M. *Eur. J. Inorg. Chem.* **2007**, in press.
(2) Delattre, J. D.; Stacy, A. M.; Siegrist, T. *J. Solid State Chem.* **2004**, *177*, 928.
(3) Gómez, M. I.; Lucotti, G., de Morán, J. A.; Aymonino, P. J.; Pagola, S.; Stephens, P.; Carbonio, R. E. *J. Solid State Chem.* **2001**, *160*, 17−24.

10.1021/cm070635y CCC: $37.00 
Published on Web 06/15/2007

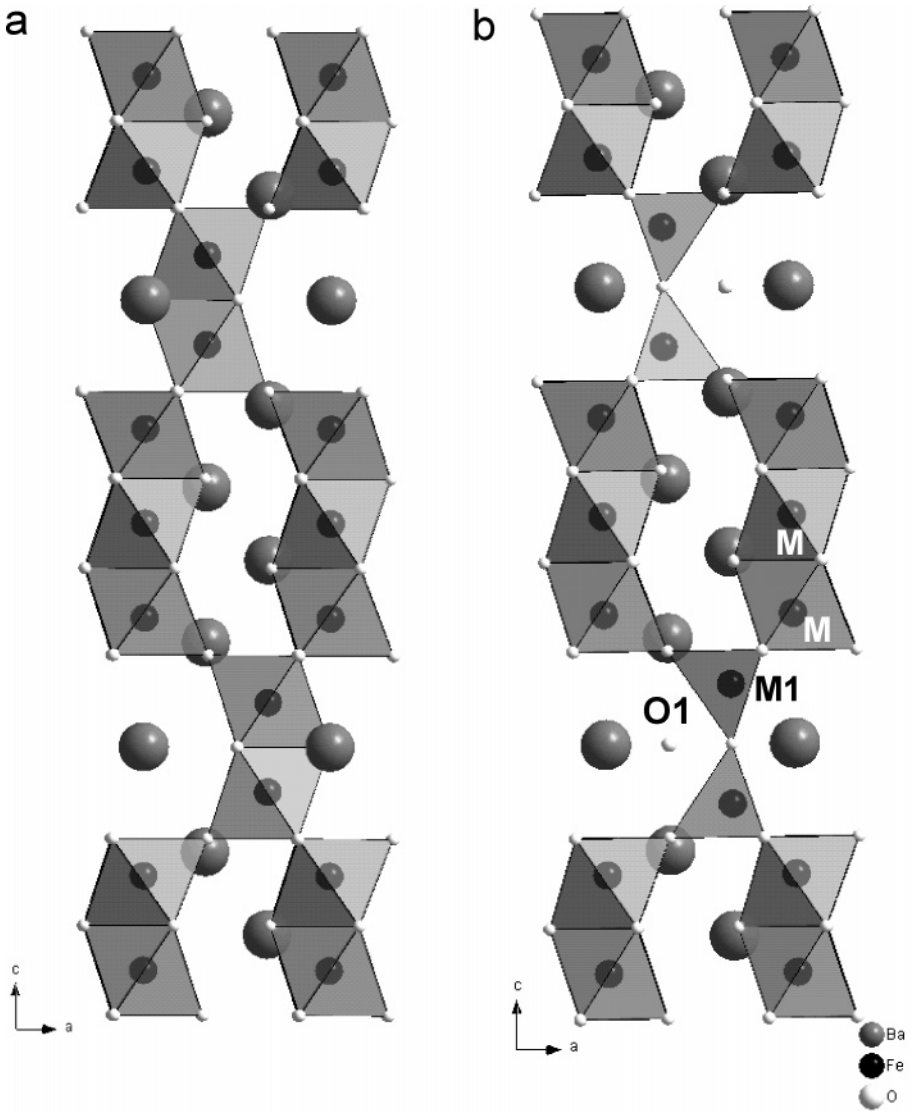


**Figure 1.** Structural models corresponding to: (a) $(hchch)_2$ 10H-$ABO_3$ polytype; (b) 10H-$BaFeO_{2.80}$ (according to ref 1). Only the M sites and nonbonding O are marked.

teristics of $BaMn_{0.4}Fe_{0.6}O_{2.73}$ have been established and show that partial substitution of Fe by Mn in $BaFeO_{2.80}$ gives rise to distinct structural differences involving both the crystal symmetry and anion vacancy distribution. In addition, ac electrical property measurements have been performed on the title compound, as there has been considerable interest in the electrical properties of cation stoichiometric[4] and/or oxygen-deficient hexagonal perovskites[5−9] in recent years. For example, several cation-stoichiometric hexagonal perovskites such as 12R-$BaTi_{1/2}Mn_{1/2}O_3$[4] and Mn-doped 6H-$BaTiO_3$[8] exhibit high permittivity values (>40) and resonate at microwave frequencies, therefore demonstrating this class of materials to be potentially interesting for microwave dielectric resonator/filter applications. Oxygen deficiency is also commonly observed in cation stoichiometric hexagonal perovskites, for example, undoped[5] and Fe-doped 6H-$BaTiO_{3-\delta}$.[9] In this case, mixed oxidation of the B-site cations occurs, e.g., $Ti^{3+}/Ti^{4+}$ in 6H-$BaTiO_{3-\delta}$, and results in semiconducting behavior due to electronic polaronic hopping on the mixed-valence B-site cation sublattice. The combination of structural and electrical characterization performed in this study therefore permits rationalization of the structure−composition−property relationships of this new hexagonal perovskite-type compound.

## Experimental Section

$BaMn_{0.4}Fe_{0.6}O_{3-y}$ was prepared by the mixed oxide route from a well-ground stoichiometric mixture of $BaCO_3$ (Aldrich, 99.98%), $MnCO_3$ (Aldrich, 99%), and $Fe_2O_3$ (Aldrich, 99.98%). The mixture was calcined in an $Al_2O_3$ crucible at 1127 K in air for 48 h then ground in a mortar and pestle and treated at 1473 K for 1 day before quenching to room temperature. This process was repeated four times with intermediate grinding to ensure homogeneity. Details of the purity, chemical composition, and oxygen content of the powder have been reported elsewhere.[1]

(4) Keith, G. M.; Kirk, C. A.; Sarma, V.; Alford, N. McN.; Cussen, E. J.; Rosseinsky, M. J.; Sinclair, D. C. *Chem. Mater.* **2004**, *16*, 2007−2015.
(5) Sinclair, D. C.; Skakle, J. M. S.; Morrison, F. D.; Smith, R. I.; Beales, T. P. *J. Mater. Chem.* **1999**, *9*, 1327−1331.
(6) Feteira, A.; Sarma, K.; Alford, N. McN.; Reaney, I. M.; Sinclair, D. C. *J. Am. Ceram. Soc.* **2003**, *86*, 511−13.
(7) Rampling, M. J.; Mather, G. C.; Marques, F. M. B.; Sinclair, D. C. *J. Eur. Ceram. Soc.* **2003**, *23*, 1911−17.
(8) Keith, G. M.; Rampling, M. J.; Sarma, K.; Alford, N. McN.; Sinclair, D. C. *J. Eur. Ceram. Soc.* **2004**, *24*, 1721−1724.
(9) Keith, G. M.; Sarma, K.; Alford, N. McN.; Sinclair, D. C. *J. Electroceram.* **2004**, *13*, 305−309.

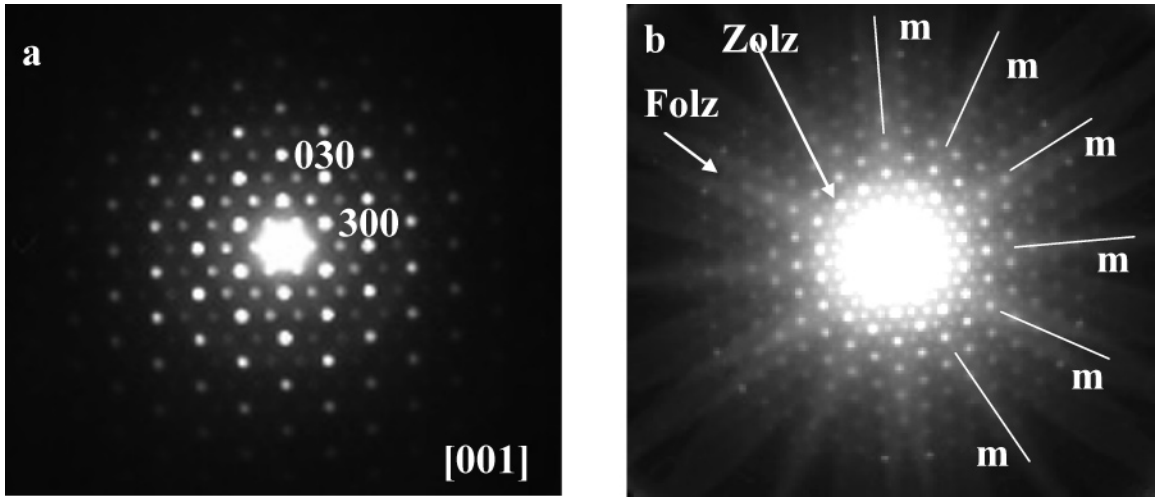


**Figure 2.** (a) SAED and (b) microdiffraction pattern along [001] for $BaMn_{0.4}Fe_{0.6}O_{2.73}$.

Electron microdiffraction was performed in a JEOL 2000FX electron microscope, fitted with a double tilting goniometer stage (±45° ±45′). Scanning electron microscopy (SEM) was performed on Au-coated as-prepared pellet surfaces using a JSM-6336F FEG SEM microscope operating at 10 kV.

Neutron powder diffraction (NPD) data were collected at room temperature on the high-resolution powder diffractometer D2B at the Institute Laue Langevin (ILL), Grenoble, France, with neutrons of wavelength 1.594 Å and covering a two theta range from 0 to 160° (step size 0.05°). Diffraction data were analyzed by the Rietveld method[10] using the Fullprof program.[11]

Powder was milled using a mortar and pestle and uniaxially pressed (Specac, Kent, UK) into cylindrical (∅ = 5 mm) pellets under an applied pressure of ∼50 MPa and then isostatically pressed (model CIP 32330, Flow Autoclave System Inc., Columbus, OH) at 200 MPa. Pellets were sintered in air at 1523 K for 2 h and reached a ceramic density of ∼5.44 g $cm^{-3}$ (∼95% of the theoretical X-ray density). Electrodes fabricated from gold paste (T-10112, Engelhard-CLAL, Cinderford, Gloucestershire, UK) were applied to both faces of the pellets, which were sintered in air at 1073 K for 1 h to remove volatiles and harden the residue.

Electrical properties of $BaMn_{0.4}Fe_{0.6}O_{2.73}$ ceramics were investigated in the temperature range 10−300 K using a cryocooler coupled to an LCR bridge (model HP 4284, Hewlett-Packard, Palo Alto, CA) and to an impedance analyzer (model HP 4192A, Hewlett-Packard, Palo Alto, CA) for fixed frequency and impedance spectroscopy measurements, respectively. All impedance data were corrected for sample geometry and analyzed using the commercial software package Z-view (Scribner Associates, Inc., Charlottesville, VA, version 2.1).

## Results and Discussion

The basic crystal structure of $BaMn_{0.4}Fe_{0.6}O_{2.73}$, obtained from XRD, electron diffraction, and high-resolution electron microscopy data, corresponds to the regular 10H $(hchch)_2$ hexagonal polytype. As mentioned in the introduction, the anion deficiency in $BaFeO_{2.80}$ is accommodated by the formation of two h′-$BaO_2$ hexagonal layers per unit cell according to a $(hch'ch)_2$ sequence.[2,3] A displacement of barium and oxygen atoms in these $BaO_2$ layers from hexagonal special positions lowers the symmetry from hexagonal to orthorhombic.[2] As this subtle structural distortion does not alter the orthohexagonal cell from the ideal axis ratio, it does not introduce significant differences in powder XRD patterns. To elucidate whether or not this symmetry change is present in $BaMn_{0.4}Fe_{0.6}O_{2.73}$, we have performed an electron microdiffraction study. The crystal symmetry can be obtained from patterns with the highest net symmetry and the Bravais lattice can be determined by comparing experimental patterns with theoretical patterns given by Morniroli et al.[12]

Figure 2a depicts the whole pattern (zero-order Laue zone (ZOLZ)) and clearly shows that only diffraction maxima corresponding to a basic hexagonal cell are observed. To confirm the hexagonal symmetry, we have performed electron microdiffraction along [001] as shown in Figure 2b, in which mirror planes are observed and superimposed in the figure, suggesting *P*6*mm* symmetry. This result confirms the hexagonal symmetry of the crystal and a whole pattern (zolz + holz) symmetry of *P*6*mm*. $BaMn_{0.4}Fe_{0.6}O_{2.73}$ therefore does not have an orthorhombic distortion as observed in $BaFeO_{2.80}$.

Having established the hexagonal symmetry of the phase, we investigated the cation and anion distribution by Rietveld refinement of neutron diffraction data using the starting model (space group $P6_3/mmc$) from our previous XRD study. Initially, oxygen vacancies were accommodated in a way similar to that in $BaFeO_{2.80}$,[3] i.e., by the formation of $BaO_2$ layers with one bonding and one nonbonding oxygen atom (Figure 1b). Mn and Fe were randomly distributed over the two different octahedral (M2 and M3) and tetrahedral sites (M1) of this space group in a 40/60 ratio according to the formula $BaMn_{0.4}Fe_{0.6}O_{2.73}$. The essential features of the cation distribution were established in a preliminary refinement. Although both metals are distributed over all polyhedra, Mn shows a strong tendency to occupy the central octahedron of the trimers (M3) rather than the outer sites (M2), whereas the tetrahedral sites are mainly occupied by Fe (M1). The refined composition (Mn:Fe = 0.69) is consistent with the

(10) Rietveld, H. M. *J. Appl. Crystallogr.* **1969**, *2*, 65.
(11) Rodríguez−Carvajal, J. *Physica B* **1993**, *192*, 55.
(12) Morniroli, J. P.; Steeds, J. W. *Ultramicroscopy* **1992**, *45*, 219.

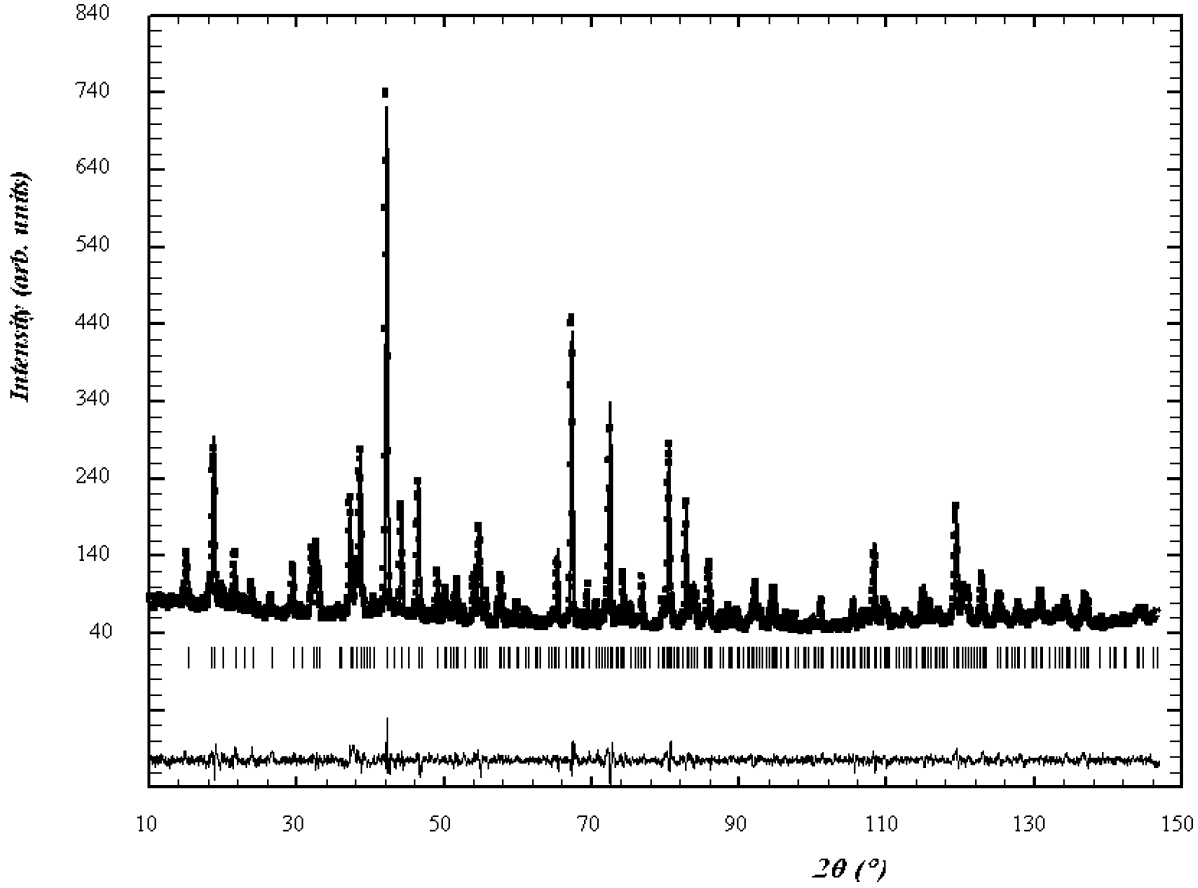


**Figure 3.** Observed, calculated, and difference profile neutron diffraction pattern for $BaMn_{0.4}Fe_{0.6}O_{2.73}$ at room temperature.

Mn:Fe experimental ratio. Having established the cation sublattice, an attempt was made to establish the oxygen sublattice.

During the early stages of the refinement, the nonbonding oxygen in the $BaO_2$ layer showed an anomalous thermal parameter with its occupancy factor tending to zero, suggesting the observed diffraction data were not consistent with an anion distribution analogous to that of $BaFeO_{2.80}$.[2] Therefore, in order to get the oxygen arrangement of $BaMn_{0.4}Fe_{0.6}O_{2.73}$, we refined the occupancy factor of all the oxygen atoms. The obtained occupation numbers did not reveal a significant concentration of oxygen vacancies in the $BaO_3$ layers forming the octahedral trimers (O2 and O3), but as in the case of $BaFeO_{2.80}$, they are confined to the O1 site at the center of the $M_2O_9$ dimers. This result proves the oxygen vacancies are correctly located in this structural block but they are distributed over the h′-$BaO_{3-y}$ layers in a different way compared to $BaFeO_{2.80}$.[3]

At this point, it is noteworthy that whereas Fe (III, IV) stabilizes both octahedral and tetrahedral oxygen environments,[2,3] in the case of Mn, the tetrahedral coordination is not likely for $Mn^{3+}$ or $Mn^{4+}$, which usually adopt square pyramidal or octahedral coordinations, respectively. As previously mentioned, the M1 site is occupied by both Mn and Fe; therefore, a new model was devised in which Fe/Mn at the M(1) site have both tetrahedral and octahedral coordination. This assumption was also made in the refinement of 5H-$BaIr_{0.2}Co_{0.8}O_{2.83}$,[13] in which a combination of both polyhedra was considered for Co/Ir in the 2d crystallographic sites of the $P\bar{3}m$ space group.

To achieve this structural model in $BaMn_{0.4}Fe_{0.6}O_{2.73,}$ the nonbonding oxygen at O1 was removed and two sites were used: O1a and O1b, forming the tetrahedra and octahedra, respectively. Simultaneous refinement of both M1 polyhedra improved the fit. The observed, calculated, and difference profile patterns of neutron diffraction data for $BaMn_{0.4}Fe_{0.6}O_{2.73}$ at room temperature are shown in Figure 3. The final structural parameters resulting from this refinement are listed in Table 1, and selected interatomic distances are given in Table 2.

A representation of the structure is given in Figure 4a. The central octahedron associated with the trimers (M3) is regular with six identical distances of 1.917 Å, whereas the outer one (M2) is distorted with three long (2.060 Å) and three short (1.893 Å) M−O distances. This distortion is caused by displacement of the metals away from the common face-sharing oxygen atoms between the M3 and M2 octahedra. This increases the M3−M2 distance and thus reduces electrostatic repulsion between cations in adjacent face-sharing polyhedra.

The Mn/Fe(1) is coordinated by either four or six oxygen atoms corresponding to tetrahedral and octahedral environments, respectively. Once again, to reduce electrostatic repulsions, we displaced the metal atoms in these polyhedra from their centers toward the c-$BaO_3$ layers. As a consequence, the in-plane O3−O3 distance, 2.968 Å, is longer than the corresponding inner and outer in-plane O−O

(13) Vente, J. F.; Battle, P. D. *J. Solid State Chem.* **2000**, *152*, 361−373.

**Table 1. Structural Parameters from the Refinement of Neutron Diffraction Data for $BaMn_{0.4}Fe_{0.6}O_{2.73}$[a]**

| atoms | site | *x*/*a* | *y*/*b* | *z*/*c* | occupancy | $B_{iso}$ (Å$^2$) |
|---|---|---|---|---|---|---|
| Ba1 | 2b | 0 | 0 | 0.25 | 1 | [b] |
| Ba2 | 4f | 1/3 | 2/3 | 0.1322(2) | 1 | 0.86(7) |
| Ba3 | 4f | 1/3 | 2/3 | 0.5407(2) | 1 | 1.25(8) |
| M1 | 4f | 1/3 | 2/3 | 0.67950(16) | 0.893(4)Fe/0.106(4)Mn | 2.06(8) |
| M2 | 4a | 0 | 0 | 0.1085(2) | 0.549(3)Fe/0.450(3)Mn | 0.37(1) |
| M3 | 2a | 0 | 0 | 0 | 0.055(6)Fe/0.943(6)Mn | 1.411(1) |
| O1a | 6h | 0.522(3) | 0.044(6) | 0.25 | 0.324(8) | [c] |
| O1b | 2d | 2/3 | 1/3 | 0.25 | 0.70(2) | [d] |
| O2 | 12k | 0.1508(5) | 0.301(1) | 0.04976(12) | 1 | 1.76(4) |
| O3 | 12k | 0.8389(6) | 0.678(1) | 0.15049(12) | 1 | 2.10(4) |

[a] Space group: $P6_3/mmc$ (194); $a = 5.74435(5)$ Å, $c = 24.0331(3)$ Å; $R_B = 6.98$, $R_{exp} = 4.14$, $\chi^2$=2.12. [b] Anisotropic temperature factors for Ba1: $\beta_{11} = 0.025(4)$, $\beta_{22} = 0.025(4)$, $\beta_{33} = 0.0023(2)$, $\beta_{12} = 0.012(2)$,$\beta_{13} = 0$, $\beta_{23} = 0$. [c] Anisotropic temperature factors for O1a: $\beta_{11} = 0.023(8)$, $\beta_{22} = 0.07(1)$, $\beta_{33} = 0.0013(3)$, $\beta_{12} = 0.034(6)$, $\beta_{13} = 0$, $\beta_{23} = 0$. [d] Anisotropic temperature factors for O1b: $\beta_{11} = 0.17(2)$, $\beta_{22} = 0.17(2)$, $\beta_{33} = 0.0025(6)$, $\beta_{12} = 0.09(1)$, $\beta_{13} = 0$, $\beta_{23} = 0$.

**Table 2. Selected Interatomic Distances (Å) in $BaMn_{0.4}Fe_{0.6}O_{2.73}$**

| | | | |
|---|---|---|---|
| Ba1−O1a | 2.88(2) × 6 | M1−M1 | 3.3898(5) |
| Ba1−O1b | 3.32(2) × 3 | M1−M2 | 3.729(3) |
| Ba1−O3 | 2.879(3) × 6 | M2−M3 | 2.609(6) |
| Ba2−O1a | 3.39(2) × 3 | M1−O1a | 2.22(2) × 3 |
| Ba2−O2 | 2.689(5) × 6 | M1−O1b | 1.694(4) |
| Ba2−O3 | 2.906(6) × 6 | M1−O3 | 1.850(6) × 3 |
| Ba3−O2 | 2.885(4) × 6 | M2−O2 | 2.060(6) × 3 |
| Ba3−O2 | 2.834(5) × 3 | M2−O3 | 1.893(6) × 3 |
| Ba3−O3 | 3.146(6) × 3 | M3−O2 | 1.917(5) × 6 |
| | | O3−O3 | 2.968(8) × 2 |
| | | O3−O3 | 2.776(8) × 2 |
| | | O2−O2 | 2.596(7) × 2 |

distances associated with the trimers, O2−O2 = 2.596 Å and O3−O3 = 2.776 Å, respectively. The polyhedral units associated with the M1 sites are therefore distorted.

The fractional occupancies of the oxygen (O1a and O1b) lead to an average $BaO_{1.65}$ composition for the oxygen-deficient h′ layers that, according to the $(hch'ch)_2$ sequence, gives rise to an oxygen content corresponding to 2.73 per formula unit, which is in excellent agreement with that obtained by TGA analysis.[1] The central octahedron of the trimers is occupied almost exclusively by Mn (94.3%), whereas Fe and Mn are present in equal amounts (∼50%) on the M2 sites within the trimers; the M1 sites are occupied mainly by Fe (89.3%). From the fractional occupancy of the O1b/O1a sites, the tetrahedral/octahedral ratio involving this crystallographic position is calculated to be 70/30; therefore, if the tetrahedral sites are fully occupied by Fe, the following cation distribution is obtained: $Ba[(Mn_{0.19}Fe_{0.011})_{Oh}]_{M3}[(Mn_{0.18}Fe_{0.22})_{Oh}]_{M2}[(Mn_{0.043}Fe_{0.077})_{Oh}(Fe_{0.280})_{td}]_{M1}O_{2.73}$, i.e., $BaMn_{0.41(1)}Fe_{0.59(2)}O_{2.73(2)}$, which agrees well with the composition established by chemical analysis.

The above results show that partial substitution of Fe by Mn in 10H-$BaFeO_{2.8}$[2,3] gives rise to distinct structural changes. Both compounds maintain the basic structural characteristics of the 10H-polytype with $(hchch)_2$ stacking but, unlike $BaFeO_{2.8}$, the crystal symmetry of $BaMn_{0.4}Fe_{0.6}O_{2.73}$ remains hexagonal. Both compounds accommodate anion deficiency by the formation of hexagonal $BaO_{3-y}$ layers in the center of the dimers but the deficiency is distributed in different ways. The distribution of anion vacancies in $BaFeO_{2.8}$ leads to the formation of corner sharing dimers only, whereas in $BaMn_{0.4}Fe_{0.6}O_{2.73}$, there is a random distribution of corner-sharing tetrahedral dimers and face-sharing octahedral dimers. The presence of such disorder is reflected in the thermal factors for barium and oxygen constituting the non-close-packed $BaO_{1.65}$ layer. In this sense, the anisotropic thermal factors for Ba1, O1a, and O1b atoms have been refined; the ellipsoids are shown in Figures 4a−c, respectively. These anisotropic thermal factors reveal the local disorder due to the presence of the large number of oxygen vacancies in the $BaO_{1.65}$ layer. In particular, the high value in the *xy* plane observed for O1b (Figure 4c) indicates significant delocalization of this atom around its mean position. Such behavior has also been observed for 5H-$BaIr_{0.2}Co_{0.8}O_{2.83}$,[13] $Ba_5Er_2Al_2ZrO_{13}$,[14] and for 10H-$BaFeO_{2.65}$;[3] in all these cases, the presence of significant anion disorder gives rise to anomalous thermal parameters.

The typical ceramic microstructure of $BaMn_{0.4}Fe_{0.6}O_{2.73}$ fired in air at 1523 K for 2 h is illustrated in Figure 5. The SEM micrograph of the as-fired surface reveals a ceramic body consisting essentially of randomly oriented anisometric plate-like grains and residual open porosity, which is in reasonable agreement with a measured ceramic density of ∼95% of the theoretical X-ray density. There is considerable variation in the grain size within the microstructure; however, in general, grains are in the size range ∼2−10 $\mu$m and often exhibit anisometric aspect ratios of ∼2−3:1. Such plate-like microstructures are commonly observed in ceramic microstructures of hexagonal-type perovskites.[15−17] A detailed microstructural evolution of Ga-doped hexagonal $BaTiO_3$ ceramics is given by Feteira et al.[17] They observed three distinctive microstructures depending on the sintering temperatures and time. Microstructures consisting of randomly orientated equiaxed grains, within a narrow grain size distribution resembling the initial particle distribution, were observed at low sintering temperatures. Necking between grains was also visible and is consistent with the low relative density (∼92%) achieved. With increasing sintering temperature/time, this microstructure was gradually replaced by a bimodal microstructure consisting of some large anisotropic

(14) Shpanchenko, R. V.; Abakumov, A. M.; Antipov, E. V.; Nistor, L.; Van Tendeloo, G.; Amelinckx, S. *J. Solid State Chem.* **1995**, *118*, 180−192.
(15) Rawal, R.; Feteira, A.; Sarma, K.; Alford, N. McN.; Sinclair, D. C. *J. Am. Ceram. Soc.* **2006**, *89*, 332−335.
(16) Rawal, R.; Feteira, A.; Arenas Flores, A.; Arma, K.; Alford, N. McN.; Hyatt, N. C.; West, A. R.; Sinclair, D. C. *J. Am. Ceram. Soc*. **2006**, *89*, 336−339.
(17) Feteira, A.; Sinclair, D. C.; Reaney, I. M. *J. Am. Ceram. Soc.* **2006**, *8*, 2105−2113.
(18) Morrison, F. D.; Sinclair, D. C.; West, A. R. *J. Am. Ceram. Soc*. **2001**, *84*, 531−38.

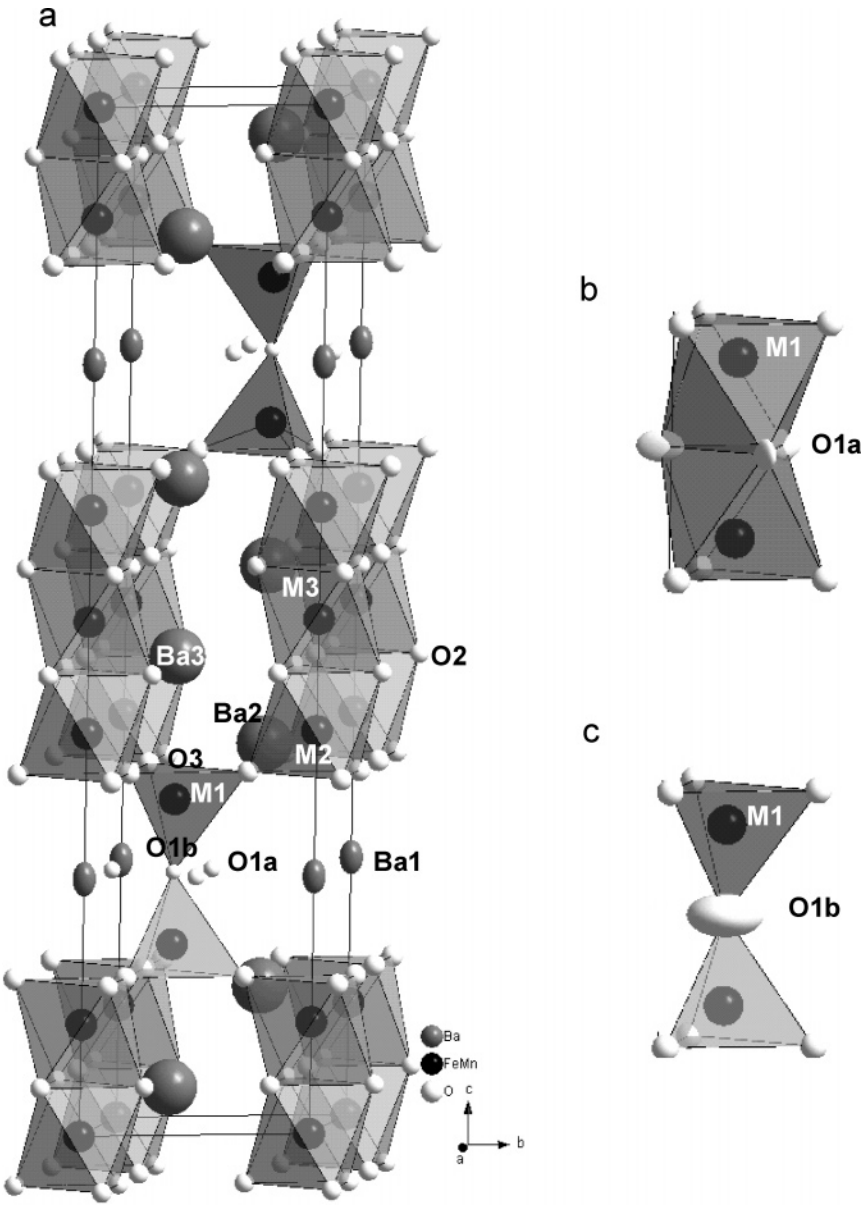


**Figure 4.** (a) Schematic representation of the structure of $BaMn_{0.4}Fe_{0.6}O_{2.73}$. The anisotropic thermal ellipsoids for (a) Ba1, (b) O1a, and (c) O1b reveal the local disorder in the non-close-packed $BaO_{1.65}$ layer.

grains embedded into a fine grained matrix, eventually reaching a microstructure consisting essentially of anisotropic grains as observed for $BaMn_{0.4}Fe_{0.6}O_{2.73}$ ceramics. In the case of $BaMn_{0.4}Fe_{0.6}O_{2.73}$ ceramics, it is worth noting the relatively poor intergranular connectivity, as this may affect the electrical response as discussed latter.

The temperature dependence of $\epsilon_r$ for $BaMn_{0.4}Fe_{0.6}O_{2.73}$ ceramics measured at 1 kHz, 10 kHz, 100 kHz, and 1 MHz in the temperature range 10−300 K is shown in Figure 6. Between 10 and 100 K, $\epsilon_r$ is essentially frequency independent and shows a small positive temperature coefficient; however, above 100 K, $\epsilon_r$ rises significantly and exhibits frequency dependent behavior, with $\epsilon_r$ decreasing with increasing frequency. For example, $\epsilon_r$ decreases from ∼56 at 10 kHz to ∼33 at 1 MHz at 300 K. The origin(s) for the apparent rise in $\epsilon_r$ at temperatures above 100 K and its frequency dependency were studied by impedance spectroscopy (IS). A selection of IS data plots obtained for $BaMn_{0.4}Fe_{0.6}O_{2.73}$ ceramics in the temperature range 10−320 K are given in Figure 7a−c.

Variation of the parallel capacitance, $C_p$, with frequency at fixed temperatures is shown in Figure 7a. At 100 K, $C_p \approx 1.6$ pF cm$^{-1}$ is frequency independent between 1 kHz and 1 MHz and is consistent with bulk behavior ($C_b$). At 300 K, $C_p$ decreases continuously from ∼ 4.7 pF cm$^{-1}$ at 10 kHz to reach 2.8 pF cm$^{-1}$ at 1 MHz. This dispersion becomes more evident as the temperature increases, as shown by the intermediate temperature of 200 K. Combined $Z''$, $M''$ spectroscopic plots exhibit Debye-like peaks; however, the peak maxima are not coincident in frequency and the $M''$ peak shows significant asymmetry at high frequency (Figure 7b). Using $<C_b = 1/2M''_{max}$ and $R = 1/\omega_{max}C$, ($\omega_{max} = 2\pi f_{max}$, where $f_{max}$ is the applied frequency in hertz at the peak maximum), which hold approximately at the $M''$ peak maximum, $C \approx 3.4$ pF cm$^{-1}$ and $R \approx 1$ MΩ cm at 250 K. The complex impedance plane, $Z^*$, plots consist of a large

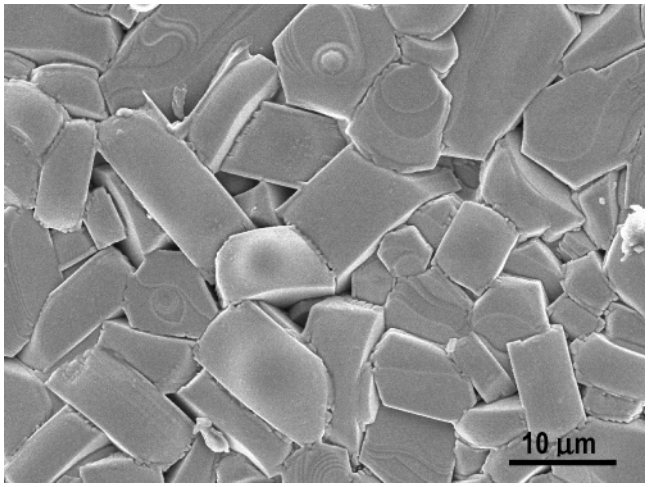


**Figure 5.** SEM micrograph of $BaMn_{0.4}Fe_{0.6}O_{2.73}$ pellet surface. The observed hexagonal and rectangular shapes correspond to the {001} and {100} crystal forms, respectively.

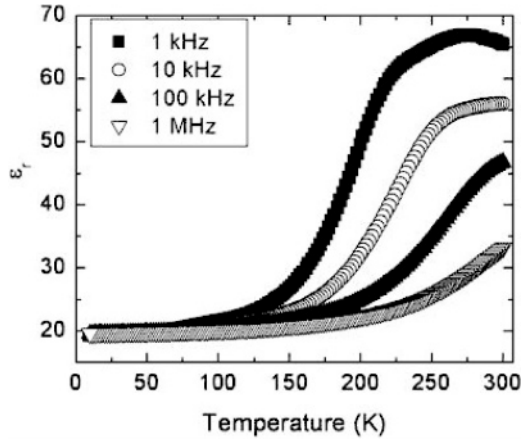


**Figure 6.** $\epsilon_r$ vs temperature at selected radio frequencies for $BaMn_{0.4}Fe_{0.6}O_{2.73}$ ceramics.

arc with an associated capacitance of a few pF $cm^{-1}$; however, there is also some asymmetry associated with the arc, as shown in Figure 7c. The low-frequency intercept with the $Z'$ axis (Figure 7c) gives the total dc resistance ($R_T$) of the sample, and the overall conductivity, $\sigma$ ($\sigma = 1/R_T$), for $BaMn_{0.4}Fe_{0.6}O_{2.73}$ ceramics is plotted against reciprocal temperature in Arrhenius format in Figure 8. The data show the ceramics to be semiconducting near room temperature and reasonable linearity is observed over the measured temperature range with an activation energy, $E_a$, for conduction of ∼0.32 eV.

IS analysis show the bulk capacitance below 100 K to be ∼1.6 pF $cm^{-1}$, which corresponds to $\epsilon_r \approx 18$ and therefore is in good agreement with the fixed frequency data below 100 K. From this data, it is clear that $BaMn_{0.4}Fe_{0.6}O_{2.73}$ ceramics have bulk permittivity <20. The apparent increase of $\epsilon_r$ at temperatures above ∼100 K observed from fixed-frequency capacitance measurements may be explained as an extrinsic effect associated with the electrically heterogeneous microstructure of the ceramics as opposed to an intrinsic effect associated with the bulk response. Similar behavior has been reported in recent years for several centrosymmetric perovskites or related materials, such as

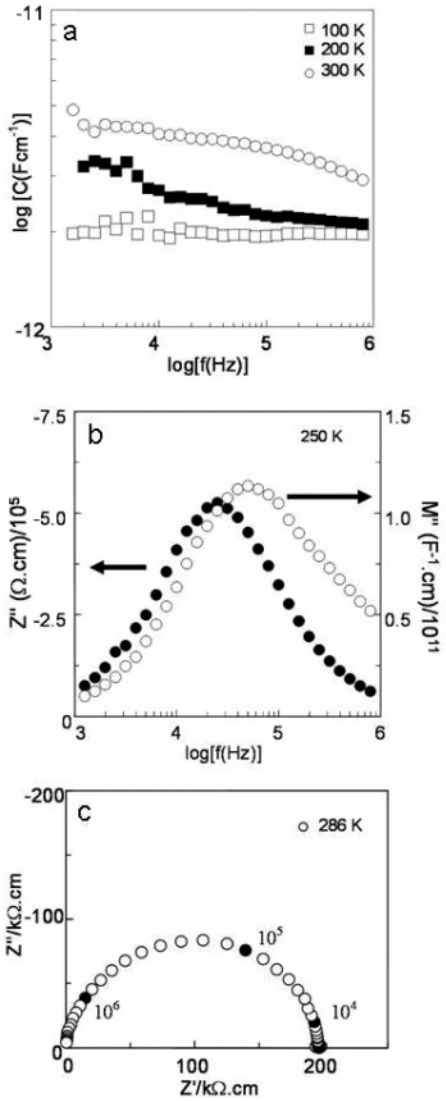


**Figure 7.** (a) $C_p$ vs frequency at 100, 200, and 300 K, (b) combined $Z''$ and $M''$ spectroscopic plot at 250 K, and (c) $Z^*$ plot at 286 K for $BaMn_{0.4}Fe_{0.6}O_{2.73}$ ceramics.

$(Ba,La,Ca)(Mn,Ti)O_3$[19] and $CaCu_3Ti_4O_{12}$,[20] and the increase in apparent permittivity has been successfully attributed to an internal barrier layer capacitance (IBLC) effect. Although the associated capacitance from the $M''$ and $Z^*$ data give a bulk-type value of ∼3−4 pF $cm^{-1}$, the nonideal Debye-like $M''$ spectroscopic plots, asymmetric $Z^*$ plots and frequency dependence of $C_p$ at >100 K all indicate that the IS data cannot be modeled on a single parallel RC element to represent an electrically homogeneous bulk response.

There are two plausible explanations for the nonideal behavior. First, the grains are electrically heterogeneous and consist of conducting cores and more resistive outer grain regions (core−shell model). This may be associated with the development of oxygen-concentration gradients between the grain and grain boundary regions in the sintered ceramics, as oxygen nonstoichiometry is known to occur in this phase. Second, a constriction resistance associated with incomplete

(19) Li, M.; Feteira, A.; Sinclair, D. C. *J. Appl. Phys.* **2005**, *98*, 084101−6.
(20) Sinclair, D. C.; Adams, T. B.; Morrison, F. D.; West, A. R. *Appl. Phys. Lett.* **2002**, *80*, 2153−2155.

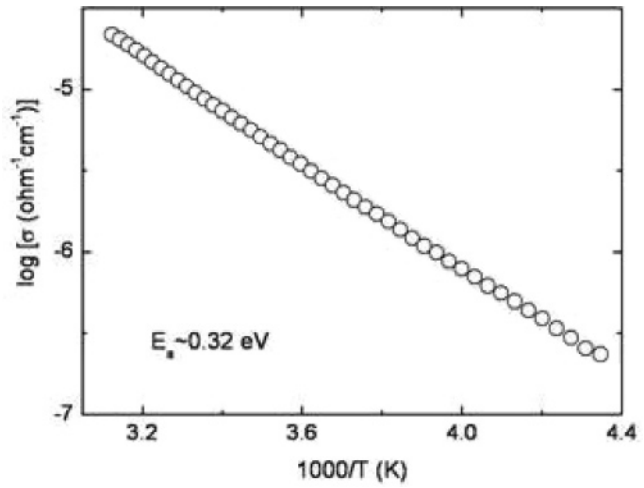


**Figure 8.** Arrhenius plot of conductivity for $BaMn_{0.4}Fe_{0.6}O_{2.73}$ ceramics.

sintering/poor grain connectivity (Figure 5) or a grain boundary phase not observed by SEM may be present in the ceramics. These regions may have a composition similar to that of the grains but they have a lower volume fraction and therefore have a time constant (RC product) similar to that of the bulk response. Although it is difficult to establish whether either (or both) explanation is correct, the IS results demonstrate that the increase in $C_p$ and therefore $\epsilon_r$ at >100 K is associated with an extrinsic (IBLC) effect and that $BaMn_{0.4}Fe_{0.6}O_{2.73}$ ceramics have bulk permittivity of <20. This permittivity value is considerably lower than that observed for other Ba-based cation stoichiometric hexagonal perovskites such as undoped and doped 6H-$BaTiO_3$[6−9] and 12R-$BaTi_{1/2}Mn_{1/2}O_3$.[4] This may be understood on the basis of the Clausius−Mossotti equation that shows the permittivity to be related directly to the sum of the ion polarizability of the ions in the unit cell and inversely to the unit cell molar volume. Fe and Mn have lower ion polarizibility compared to Ti[21] and the normalized "thickness" of the $BaO_3$ close-packed layers, estimated by the ratio $c/N$ (where $c$ = $c$-axis length, $N$ = number of close packed layers in the unit cell) is 2.40331 Å for $BaMn_{0.4}Fe_{0.6}O_{2.73}$ compared to 2.327 Å for 12R-$BaTi_{1/2}Mn_{1/2}O_3$[4] and 2.328 Å for 6H-$BaTiO_3$.[5] The larger $c/N$ for $BaMn_{0.4}Fe_{0.6}O_{2.73}$ can be attributed to a combination of the different stacking sequence of the $BaO_3$ layers in this compound (40% ccp compared to 50 and 60% ccp in 12R- and 6H-polytypes, respectively) and to increased cation−cation repulsion effects associated with the presence of oxygen vacancies.

Finally, the semiconductivity (∼5 $\mu$S $cm^{-1}$ at 300 K) and low activation energy for conduction (∼0.32 eV) is consistent with polaron hopping most probably associated with a small amount of mixed valency associated with Fe and/or Mn ions on the B-site sublattice. The conductivity is significantly higher than that observed for 12R-$BaTi_{1/2}Mn_{1/2}O_3$ (<1 nS $cm^{-1}$ at 300 K)[4] which contains negligible levels (<0.1 at %) of oxygen vacancies and therefore mixed valency of the B-site cations. The appreciable level of electronic conduction exhibited by $BaMn_{0.4}Fe_{0.6}O_{2.73}$ ceramics in comparison with 12R-$BaTi_{1/2}Mn_{1/2}O_3$ ceramics will certainly dramatically increase their dielectric losses at microwave frequencies, and it can be anticipated that resonance behavior will be inhibited.

In conclusion, the 10H-type hexagonal crystal structure of $BaMn_{0.4}Fe_{0.6}O_{2.73}$ has been established and differs significantly from $BaFeO_{2.80}$. In particular, the presence of 40% Mn on the B-site results in a different distribution of the anion vacancies in the oxygen-deficient h′-$BaO_{1.65}$ layers. In $BaFeO_{2.8}$, the distribution of oxygen vacancies leads to the formation of corner-sharing tetrahedral dimers only, whereas in $BaMn_{0.4}Fe_{0.6}O_{2.73}$, a random distribution of Fe-containing corner-sharing tetrahedral dimers and mixed Fe/Mn-containing face-sharing octahedral dimers occurs. The compound is a leaky insulator at room temperature with a permittivity of ∼20. The conduction mechanism has a low activation energy and is consistent with polaronic hopping associated with the Fe and/or Mn ions.

**Acknowledgment.** Financial support through research project MAT2004-01248 (Madrid), FAME-EU (Madrid, Sheffield), and EPSRC (Sheffield) is acknowledged.

CM070635Y

(21) Shannon, R. D. *J. Appl. Phys.* **1993**, *73*, 348−366.